Supporting Information

Improved Electrochemical Performance and Capacity Fading Mechanism of Nano-sized $LiMn_{0.9}Fe_{0.1}PO_4$ Cathode Modified by Polyacene Coating

Liguang Wang[a], Pengjian Zuo[a], Yulin Ma[a], Xinqun Cheng[a], Chunyu Du[a], Geping Yin[a] and Yunzhi Gao[a]*

[a]School of Chemical Engineering and Technology, Harbin Institute of Technology, No.92 West-Da Zhi Street, Harbin 150001, China

*Corresponding Author: E-mail: zuopj@hit.edu.cn, zuopjhit@gmail.com (P. Zuo)

Tel./fax: +86-451-86403216

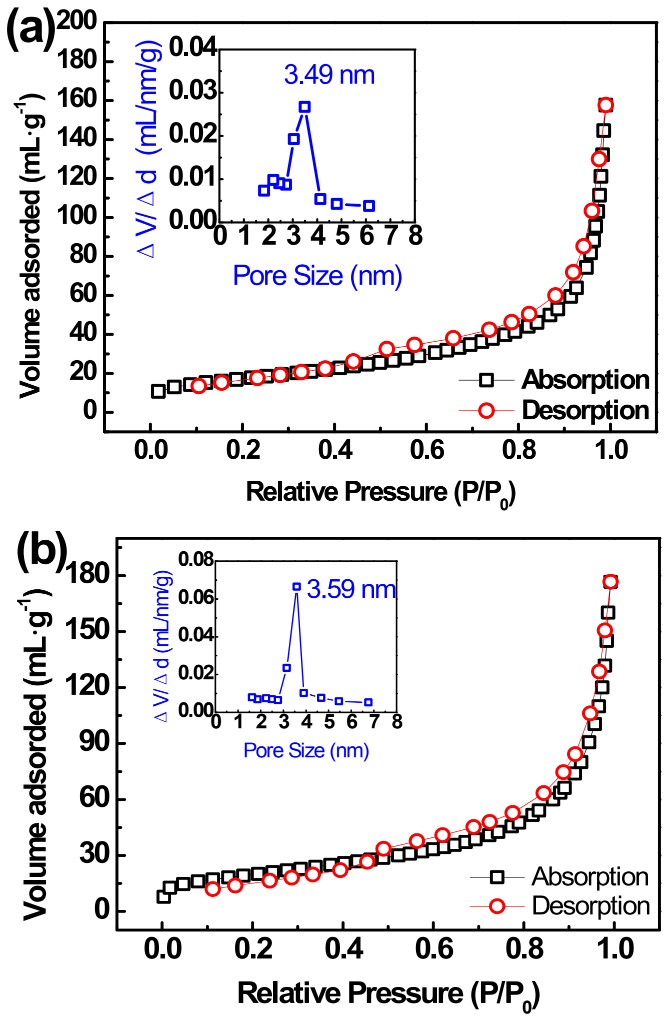

Figure S1. Nitrogen sorption isotherm with pore size distribution (inset) and $LiMn_{0.9}Fe_{0.1}PO_4$-PAS.

The porous structure and the BET surface area of $LiMn_{1-x}Fe_xPO_4$-PAS (x = 0 and 0.1) composite were investigated by N_2 adsorption-desorption experiments at 77K (Figure S1). The BET surface area measured is 65.6 and 71.5 $m^2 \cdot g^{-1}$ for $LiMnPO_4$-PAS and $LiMn_{0.9}Fe_{0.1}PO_4$-PAS, respectively. The average pore diameter is 3.49 and 3.59 nm for $LiMnPO_4$-PAS and $LiMn_{0.9}Fe_{0.1}PO_4$-PAS, respectively, which is calculated using the Barrett-Joyner-Halenda (BJH) method. The high surface area and the small average pore will facilitate the diffusion of Li^+ in the olivine-type $LiMnPO_4$ class of materials.

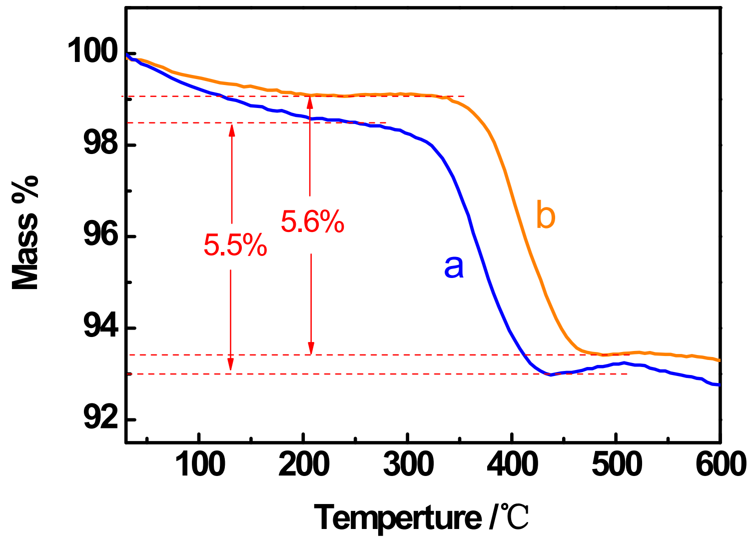

Figure S2. TG curves of (a) $LiMnPO_4$-PAS and (b) $LiMn_{0.9}Fe_{0.1}PO_4$-PAS.

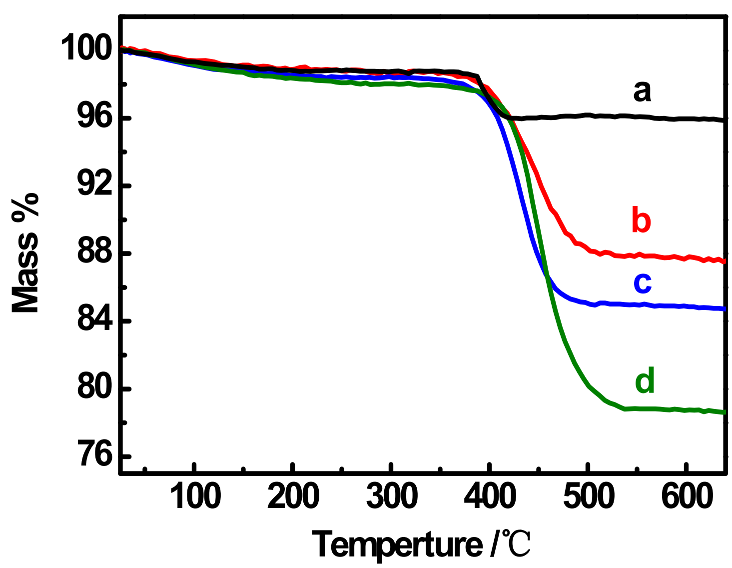

Figure S3. $LiMn_{0.9}Fe_{0.1}PO_4$-PAS samples recorded with a heating rate of 10℃·min^{-1} in an oxygen atmosphere with different amount of PAS: (a) 3 wt%, (b) 11 wt%, (c) 15 wt% and (d) 20 wt%.

The PAS contents in $LiMn_{0.9}Fe_{0.1}PO_4$-PAS powders were estimated by thermogravimetric (TG) measurement of the PAS coated $LiMn_{0.9}Fe_{0.1}PO_4$ products in oxygen atmosphere (Figure S3). The weight loss below 200℃ is due to the evaporation of adsorbed moisture. It can be seen that the maximum weight loss of the samples locates at 300-500℃, which is contributed to the PAS of the composite. By neglecting the tiny deviation, the PAS contents of $LiMn_{0.9}Fe_{0.1}PO_4$-PAS powders were estimated 3 wt%, 5.6 wt%, 11 wt%, 15 wt% and 20 wt%, respectively.

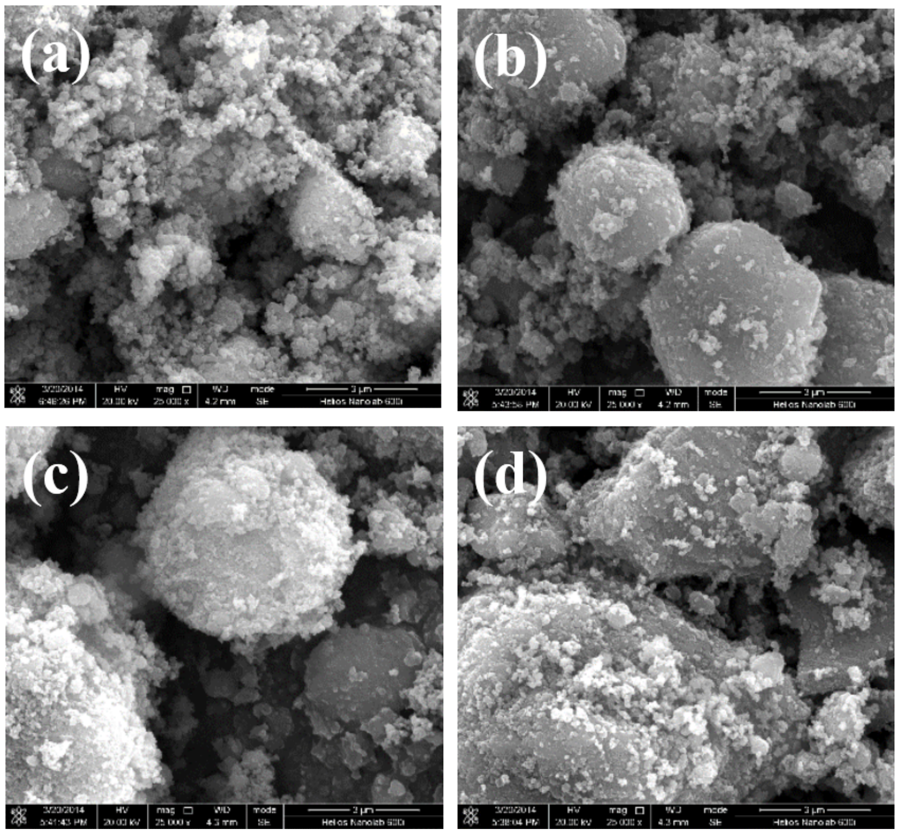

Figure S4. SEM images of $LiMn_{0.9}Fe_{0.1}PO_4$-PAS powders with different amount of PAS: (a) 3 wt%, (b) 11 wt%, (c) 15 wt% and (d) 20 wt%.

The PAS content of $LiMnPO_4$-PAS and $LiMn_{0.9}Fe_{0.1}PO_4$-PAS was 5.5 wt% and 5.6 wt%, respectively (Figure S2). From Figure S3 and S4, it can be seen that the increasing PAS content made agglomeration exacerbated, which reduced the conductivity of the materials (Table S1). While the 3wt% PAS in the composite cannot supply the integrated conducting layer on the surface of nanoplates and the conductive network among the particles, resulting in the low conductivity of the composite. Therefore, the $LiMn_{0.9}Fe_{0.1}PO_4$-PAS composite with 5.6 wt% PAS exhibited the largest electrical conductivity.

Table S1. Conductivity of $LiMn_{0.9}Fe_{0.1}PO_4$-PAS powders with different amount of PAS.

Samples	**3 wt% ($S\cdot cm^{-1}$)**	**5.6 wt% ($S\cdot cm^{-1}$)**	**11 wt% ($S\cdot cm^{-1}$)**	**15 wt% ($S\cdot cm^{-1}$)**	**20 wt% ($S\cdot cm^{-1}$)**
Conductivity	1.2×10^{-2}	1.5×10^{-1}	6.8×10^{-2}	5.4×10^{-2}	3.8×10^{-2}

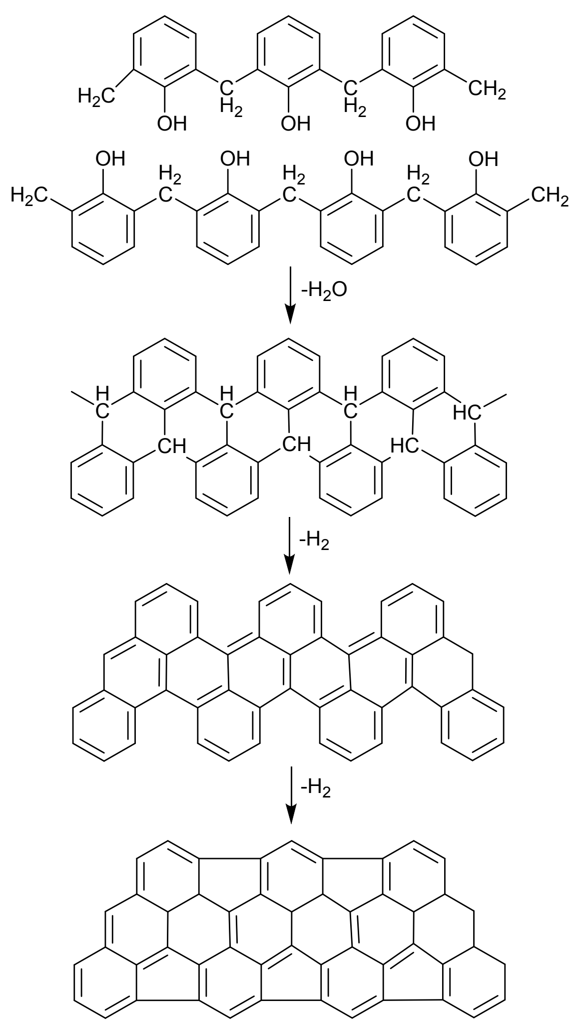

Figure S5. The formation process of PAS. During the process, phenolic resin was dehydrated and dehydrocyclized as temperature increases and the final product was PAS.[1]

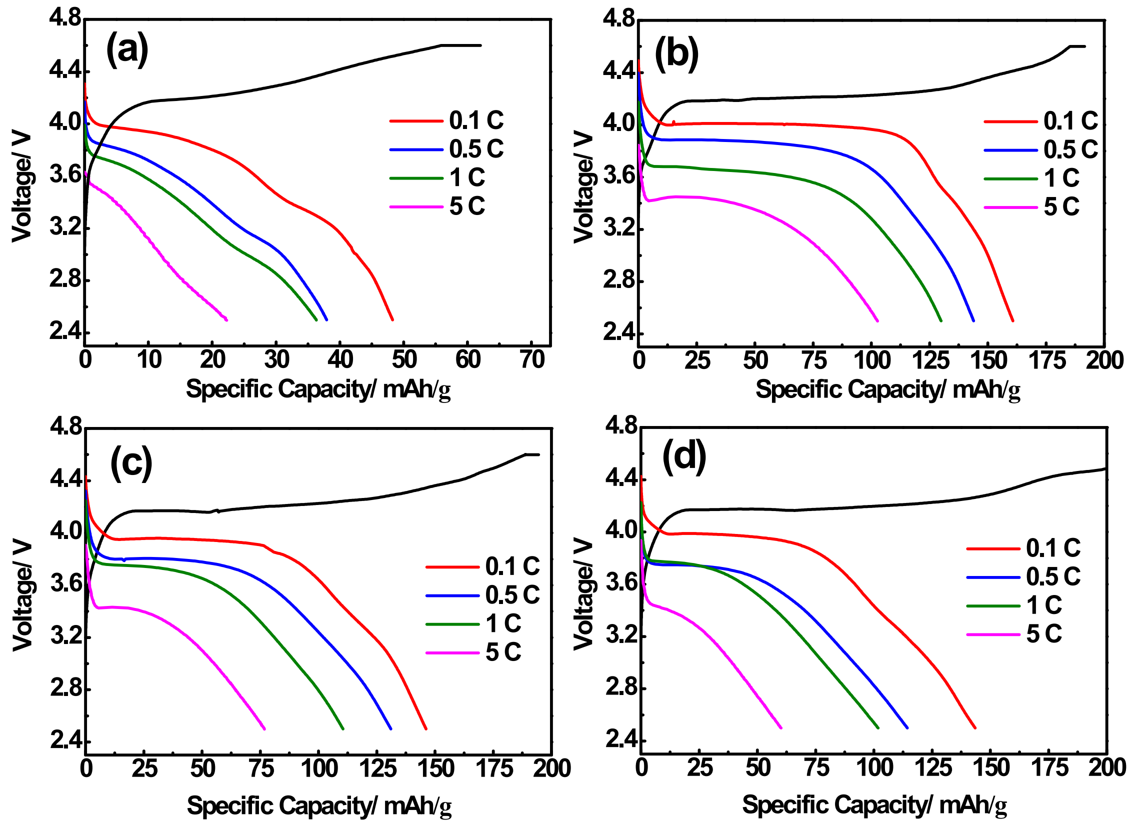

Figure S6. Initial charge/discharge curves of $LiMn_{0.9}Fe_{0.1}PO_4$-PAS with different .amount of PAS: (a) 3%, (b) 11%, (c) 15% and (d) 20%.

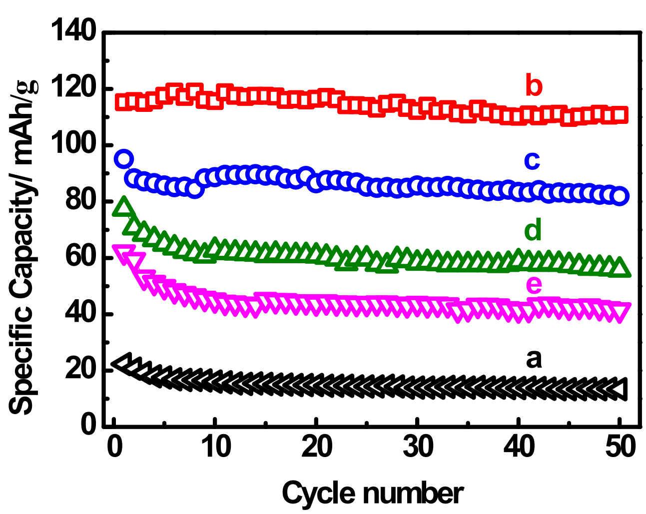

Figure S7. Cycling stability of Li/$LiMn_{0.9}Fe_{0.1}PO_4$-PAS cells with different amounts of PAS at 5 C rate: (a) 3%, (b) 5.6%, (c) 11%, (d) 15% and (e) 20%.

To determine the optimal carbon content of the composites, the $LiMn_{0.9}Fe_{0.1}PO_4$ cells with various amounts of PAS (3 wt% to 20 wt%) were prepared. Figure S6 shows the initial charge/discharge curves of the samples. The discharge capacities of the $LiMn_{0.9}Fe_{0.1}PO_4$-PAS manifestly increase with increasing PAS content up to 11 wt%, which is 48 $mAh \cdot g^{-1}$ at 3 wt%, 160.7 $mAh \cdot g^{-1}$ at 5.6 wt% and 157 $mAh \cdot g^{-1}$ at 11 wt% at 0.1 C. For the samples with 15 wt% PAS and 20 wt% PAS, the discharge capacities drop to 146 and 143.5 $mAh \cdot g^{-1}$, respectively. The decreased discharge capacity can be attributed to the growth in the charge-transfer resistance caused by the excessive presence of electrochemically inactive PAS and the agglomeration during pyrolysis (evident in Figure S4).

Figure S7 illustrates cycling stability of Li/$LiMn_{0.9}Fe_{0.1}PO_4$-PAS cells with different amounts of PAS at 5 C rate discharge. The highest specific capacity at the 5 C rate is obtained from the $LiMn_{0.9}Fe_{0.1}PO_4$-PAS composite with 5.6 wt % of PAS. After 50 cycles, this composite retains 111 $mAh \cdot g^{-1}$, corresponding to 96.5% of its first discharge capacity, which is much higher than others. The electrochemical cycling data in Figure S6 are consistent with the microstructure and EIS results (Figure S8). From the Figure S8, we can see that the $LiMn_{0.9}Fe_{0.1}PO_4$-PAS composite with 5.6 wt % PAS has the smallest R_{ct} and the largest D, which is agree well with the electrochemical performance. The strong adhesion conducting PAS layer on the surface of $LiMn_{0.9}Fe_{0.1}PO_4$ nanoplates and the well-distributed conducting wrinkled PAS nanoplates surrounding the $LiMn_{0.9}Fe_{0.1}PO_4$ particles form a network of electrically conducting paths for electrons. Meanwhile, the smaller $LiMn_{0.9}Fe_{0.1}PO_4$-PAS particles shorten the diffusion length for the Li^+ ions. Therefore, the electrode with 5.6 wt% PAS is expected to deliver the best electrochemical performance.

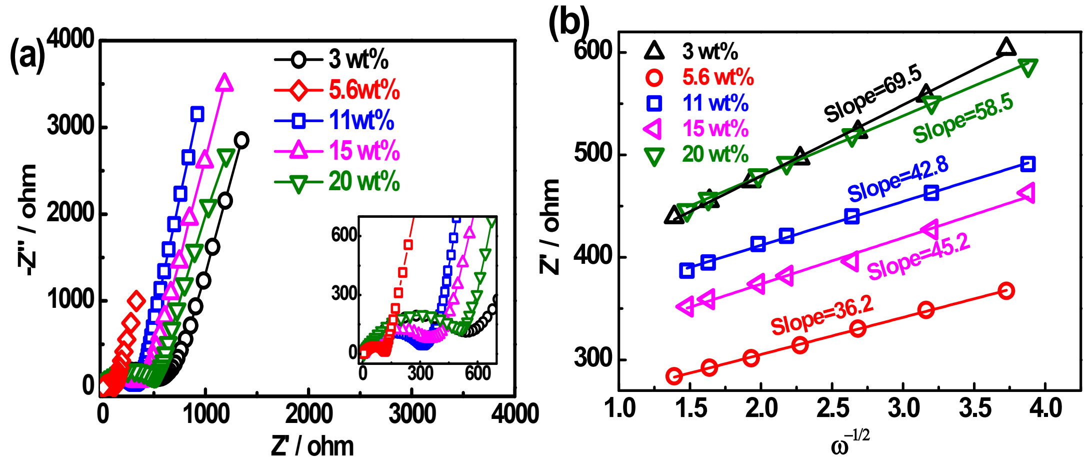

Figure S8. Nyquist plots of Li/ $LiMn_{0.9}Fe_{0.1}PO_4$-PAS cells with different amounts of PAS (a); the relationship plot of Z′ vs. $\omega^{-1/2}$ at low-frequency region (b).

Table S2 The diffusion coefficient of the LMFP-PAS with different amounts of PAS.

Samples	3 wt%	5.6 wt%	11 wt%	15 wt%	20 wt%
D(cm^2/s)	6.34×10^{-15}	2.34×10^{-14}	1.67×10^{-14}	1.50×10^{-14}	6.34×10^{-15}

REFERENCES

1. Trick, K. A.; Saliba, T. E., Mechanisms of the Pyrolysis of Phenolic Resin in a Carbon/Phenolic Composite. *Carbon* **1995,** *33*, 1509-1515.